©(2010) ISSN 1513-489X East-West J. of Mathematics Bangkok Thailand

a special volume 2010, pp.266-282 ICMA-MU 2009 proceedings

A Variational Approach for Discontinuity-Preserving Image Registration

Noppadol Chumchob[1], Ke Chen[1]

[1]Centre for Mathematical Imaging Techniques, Department of Mathematics, The University of Liverpool, Peach Street, Liverpool L69 7ZL, United Kingdom.
n.chumchob@liv.ac.uk; k.chen@liv.ac.uk

Abstract

There exist many models for deformable image registration, mainly differing in how regularization is introduced. On one hand, models minimizing first- or second-order derivatives such as diffusion-, elastic-, or curvature-based image registration are known to generate globally smooth deformation fields. On the other hand, regularization techniques based on total variation (TV) preserving discontinuities of the deformation field are useful to a class of problems where smoothness is less a concern. It is still a challenge to design a model suitable for both smooth problems and non-smooth problems.

This talk first proposes a variational model based on a modified TV regularization, which can be interpreted as a half way model between diffusion (smooth) and TV (non-smooth) registration. The idea stems from image restoration where smoothing and preserving discontinuities are both important. Second to solve the resulting Euler- Lagrange system of two coupled, nonlinear partial differential equations (PDEs), we present a nonlinear multigrid (NMG) strategy and an adaptive parameter selection procedure. Numerical tests using both synthetic and realistic images not only confirm that the proposed model is more robust in registration quality for a wide range of applications than previous models, but also that the proposed NMG method can deliver an acceptable solution many orders of magnitude faster than the gradient descent approach, popularly used in image processing.

Keywords: deformable image registration, discontinuity-preserving image registration, non-rigid image registration, nonlinear multigrid, total variation, variational approach.

AMS Subject Classifications: 65K10, 65N55, 94A08, 47A52.

1 Introduction

Image registration, also called *image fusion*, *image matching* or *image warping*, is a widely used task in image processing and is applied whenever a series of images of the same or similar scene needs to be compared or integrated. It has applications in various fields. Particularly, in medical imaging there are practical applications that require a registration step to monitor disease progression and/or plan treatment

guidance. For an overview on registration methodology, we refer to [14, 15], and references therein. This work focuses on deformable image registration set in a variational framework [15].

Given a so-called *reference* image R and a so-called *template* image T, the goal of image registration is to determine a *reasonable* transformation φ, such that the transformed version of the template becomes similar to the reference in the geometrical sense. Here, we model the given images R and T as smooth and compactly supported functions mapping points of a rectangular domain $\Omega \subset \mathbb{R}^2$ to a domain $V \subset \mathbb{R}_0^+$ and the template is distorted by the transformation $\varphi(\mathbf{x}) = \mathbf{x} + \boldsymbol{u}(\mathbf{x})$ with a so-called *deformation* or *displacement field* $\boldsymbol{u} : \Omega \to \Omega$, whose components u_1 and u_2 are functions of the variable $\mathbf{x} = (x_1, x_2)^\top$ in the image domain Ω. The term $\boldsymbol{u}$ is used to model the transformation φ because it can view as how a point in the deformed template image $T(\boldsymbol{u}) = T(\mathbf{x} + \boldsymbol{u}(\mathbf{x})) = (T \circ \varphi)(\mathbf{x})$ is moved away from its original position. Thus the problem of estimating the transformation φ and the deformation field $\boldsymbol{u}$ are equivalent. Without loss of generality we assume that $\Omega = [0, 1]^2 \subset \mathbb{R}^2$ and $V = [0, 1]$ for 2D gray-scale images throughout this work.

As is known, deformable image registration is a nonlinear and ill-posed problem in the sense of Hadamard (i.e., uniqueness of the solution is not guaranteed). Therefore, it becomes necessary to impose a deformation model for penalising unwanted and irregular displacement fields as much as possible using some prior knowledge. In general, various variational models for the deformable image registration have two basic building blocks. The first one is a so-called *similarity measure* $\mathcal{D}$ quantifying distance or similarity of two given images R and T, and the second one is a so-called *regularizer* $\mathcal{R}$, which rules out unwanted, irregular, and/or nonunique solutions during registration process. As a consequence, the deformable image registration can be mathematically posed as a minimization problem of the so-called Tikhonov energy functional,

$$\mathcal{J}_\alpha[\boldsymbol{u}] = \mathcal{D}(R, T(\boldsymbol{u})) + \alpha \mathcal{R}(\boldsymbol{u}). \tag{1}$$

Here $\alpha > 0$ is the so-called regularization parameter that compromises similarity and regularity; Section 4 presents an idea of selecting α. When the image intensi-

ties of the given images R and T are comparable (i.e., in a monomodal registration scenario), the proper choice of $\mathcal{D}$ is the so-called *sum of squared differences* (SSD) given by

$$\mathcal{D}\left(R, T\left(\boldsymbol{u}\right)\right) = \frac{1}{2}\int_{\Omega}\left(T\left(\mathbf{x}+\boldsymbol{u}\left(\mathbf{x}\right)\right)-R\left(\mathbf{x}\right)\right)^{2}d\mathbf{x}, \tag{2}$$

which is adopted in this work.

1.1 Review of four image registration models

The actual choice of the building block $\mathcal{R}$ is very crucial and depends on the application under consideration. Different choices of $\mathcal{R}$ not only lead to different deformation models but also to different Euler-Lagrange systems involving coupled nonlinear PDEs. The most popular are the following:

(1) *Elastic image registration*, where $\mathcal{R}$ is based on the linearised elastic potential and given by

$$\mathcal{R}^{\text{elas}}(\boldsymbol{u}) = \int_{\Omega}((\mu/4)\sum_{l,m=1}^{2}(\partial_{x_l}u_m+\partial_{x_m}u_l)^2+(\lambda/2)(\nabla\cdot\boldsymbol{u})^2)d\mathbf{x}. \tag{3}$$

Here $\mu > 0$ and $\lambda \geq 0$ are the so-called Lamé constants which reflect material properties; see more details in [15] and references therein.

(2) *Diffusion image registration* [2, 3, 11, 12, 15, 18], where $\mathcal{R}$ is based on the first-order partial derivatives of u_l and given by,

$$\mathcal{R}^{\text{diff}}(\boldsymbol{u}) = \frac{1}{2}\sum_{l=1}^{2}\int_{\Omega}|\nabla u_l|^2\,d\mathbf{x}. \tag{4}$$

(3) *Fischer–Modersitzki's curvature image registration* [4, 9, 11, 12, 15], where $\mathcal{R}$ is based on an approximation of the mean curvature of the surface of u_l and given by

$$\mathcal{R}^{\text{curv}}(\boldsymbol{u}) = \frac{1}{2}\sum_{l=1}^{2}\int_{\Omega}(\Delta u_l)^2 d\mathbf{x}. \tag{5}$$

(4) *Total variation (TV) image registration* [5], where $\mathcal{R}$ is based on the first-order partial derivatives of u_l and given by

$$\mathcal{R}^{\beta\text{TV}}\left(\boldsymbol{u}\right) = \sum_{l=1}^{2}\int_{\Omega}|\nabla u_l|_{\beta}\,d\mathbf{x} = \sum_{l=1}^{2}\int_{\Omega}\sqrt{u_{l_{x_1}}^2+u_{l_{x_2}}^2+\beta}d\mathbf{x}. \tag{6}$$

Here $\beta > 0$ is a small real parameter for avoiding non-differentiable at zero; see more details in [5, 16].

As is known, $\mathcal{R}^{\text{elas}}$, $\mathcal{R}^{\text{diff}}$, and $\mathcal{R}^{\text{curv}}$ produce globally smooth deformation fields. While they are useful for several applications, they become poor if discontinuities or steep gradients in the deformation fields are expected (e.g. resulting from multiple moving objects or partially occluded objects). See Figures 1-2 for a particular registration problem where the common regularization techniques yield oversmooth deformation fields and Figures 3-4 for a typical registration problem requiring smooth deformation fields.

In order to preserve discontinuities of the deformation field, $\mathcal{R}^{\beta\text{TV}}$ helps to preserve piecewise constant smoothness, which is much weaker than those global smoothness of $\mathcal{R}^{\text{elas}}$, $\mathcal{R}^{\text{diff}}$, and $\mathcal{R}^{\text{curv}}$; see Figures 3-5 for example. However, $\mathcal{R}^{\beta\text{TV}}$ may not be suitable for some particular image registration problems, which require deformation fields having very strong smoothing properties, i.e. where the staircase effect is not desirable.

1.2 Review of numerical techniques for deformable image registration

Various numerical techniques for deformable image registration have been proposed in solving the Euler-Lagrange systems of coupled nonlinear PDEs resulting from the minimization problem of the energy functional (1). These technique can be broadly divided into two main categories: the so-called *parabolic* and *elliptic* approaches. A parabolic (gradient descent or time marching) approach performs by introducing the so-called artificial time variable and then determining the steady state solution of the system of time-dependent linear PDEs (see e.g. [3, 4, 9, 12, 15, 18]) and an elliptic approach performs by directly solving the system of nonlinear PDEs with a method of our choice, e.g. the fixed-point (FP) iteration, Newton-type, multigrid (MG) methods (see e.g. [2, 5, 6, 7, 8, 10, 11, 13, 19]). As is known, MG techniques are usually much faster than those of gradient descent approaches, commonly used in image processing applications. Therefore, in this paper we propose a fully automatic, fast, and accurate approach based on the so-called full approximation scheme nonlinear multigrid (FAS-NMG) strategy (see [17]) and an adaptive procedure in selecting the optimal value of α developed by [2]. In literature, the use of MG techniques for deformable image registration is

hardly new; see e.g. [2, 5, 6, 7, 8, 9, 10, 11, 18, 19] and references therein. However, the use of the FAS-NMG methods for this kind of registration problems is relatively new with a few references; see e.g. [2, 6, 8, 19]. To the best of our knowledge, it is completely new in the field of discontinuity-preserving image registration.

The rest of the paper is organized as follows. Section 2 first presents a new variational model that can helps to preserve discontinuities of $\boldsymbol{u}$ and then discusses its numerical solution based on the FAS-NMG method in Section 3. Section 4 presents a method of selecting the optimal value of α. Experimental results from syntectic and real images are illustrated in Section 5 before conclusions in Section 6.

2 A new discontinuity-preserving model

Motivated by several regularization techniques that have been prove to be very useful in optical flow computation, image reconstruction, and image restoration; see [1] and references therein, one can smooth isotropically each component of $\boldsymbol{u}$ inside homogeneous (or flat) regions corresponding to weak gradients and preserve its discontinuities in inhomogeneous regions presenting large gradients by replacing $|\nabla z|$ in (6) (where z is u_1 or u_2) by $\phi\left(|\nabla z|\right)$ where the so-called *potential function* ϕ satisfies some conditions to ensure the discontinuity-preserving. Consequently, our modified TV (MTV) model can be represented in terms of a general notation,

$$\mathcal{R}^{\mathrm{MTV}}(\boldsymbol{u}) = \sum_{l=1}^{2} \int_{\Omega} \phi\left(|\nabla u_l|\right) d\mathbf{x}, \tag{7}$$

and then leads to the nonlinear system of PDEs given by

$$\begin{cases} f_1(\boldsymbol{u}) - \alpha \nabla \cdot \left(\frac{\phi'(|\nabla u_1|)}{|\nabla u_1|} \nabla u_1\right) = 0, \qquad f_2(\boldsymbol{u}) - \alpha \nabla \cdot \left(\frac{\phi'(|\nabla u_2|)}{|\nabla u_2|} \nabla u_2\right) = 0 \\ \text{subject to } \frac{\phi'(|\nabla u_l|)}{|\nabla u_l|} \partial_{\boldsymbol{n}} u_l = 0 \text{ on } \partial\Omega \qquad \text{(MTV)} \end{cases} \tag{8}$$

where $\boldsymbol{n} = (n_1, n_2)^{\top}$ is the outward unit vector normal to the image boundary $\partial\Omega$ and

$$f_1\left(\boldsymbol{u}\right) = \left(T(\boldsymbol{u}) - R\right) \partial_{u_1} T(\boldsymbol{u}), \qquad f_2\left(\boldsymbol{u}\right) = \left(T(\boldsymbol{u}) - R\right) \partial_{u_2} T(\boldsymbol{u}) \tag{9}$$

are the results of the first variation of the data term $\mathcal{D}$.

There exist many choices for the potential function ϕ [1] to modify the TV model. Below we give some commonly used ones for (7) and its diffusion coefficient $D\left(s\right) = \phi'\left(s\right)/s$:

- $\phi(s) = \frac{1}{p}s^p$, $D(s) = \frac{1}{s^{2-p}}$, $1 < p < 2$ (ϕ is related to (6), i.e. $\mathcal{R}^{\beta\mathrm{TV}}$ when $p = 1$)
- $\phi(s) = \log\left(1 + s^2\right), D(s) = \frac{2}{1+s^2}$,
- $\phi(s) = \frac{s^2}{1+s^2}$, $D(s) = \frac{2}{(1+s^2)^2}$
- $\phi(s) = 2\sqrt{1+s^2} - 2$, $D(s) = \frac{2}{\sqrt{1+s^2}}$
- $\phi(s) = 2\log[\cosh(s)]$, $D(s) = \begin{cases} 2 & , \ s = 0 \\ 2\tanh(s)/s & , \ s \neq 0 \end{cases}$

It is worth noticing that the diffusion coefficient (or the stopping function) $D(s)$ has the following basic properties: (1) $D(s) \to 0$ as $s \to \infty$. (2) $D(s) \to M$ $(0 < M < +\infty)$ as $s \to 0$. These mean that on one hand it preserves discontinuities of $\boldsymbol{u}$ by reducing or stopping the diffusion (smoothing) process in inhomogeneous regions, on the other hand it smooths $\boldsymbol{u}$ isotropically inside homogeneous regions. In other words, TV-like regularization is used in inhomogeneous regions and diffusion- or quadratic-like regularization is used in homogeneous regions. These are the main reasons how $\mathcal{R}^{\mathrm{MTV}}$ can be simply interpreted as a half way between diffusion and TV regularization techniques for deformable image registration; see e.g. Figures 1-5. In this study, we focus only on the potential function ϕ defined by $\phi(s) = \log\left(1 + s^2\right)$ to be a numerical phototype for this kind of regularization techniques, and then the resulting Euler-Lagrange equations can be explicitly expressed in terms of the nonlinear system of two coupled PDEs as follows:

$$\begin{cases} \underbrace{f_1(\boldsymbol{u})\overbrace{-\alpha\nabla\cdot\left(\frac{2\nabla u_1}{1+(|\nabla u_1|)^2}\right)}^{\mathcal{L}_{\mathrm{NL}}(u_1)}}_{\mathcal{N}_1(\boldsymbol{u})} = g_1, \qquad \underbrace{f_2(\boldsymbol{u})\overbrace{-\alpha\nabla\cdot\left(\frac{2\nabla u_2}{1+(|\nabla u_2|)^2}\right)}^{\mathcal{L}_{\mathrm{NL}}(u_2)}}_{\mathcal{N}_2(\boldsymbol{u})} = g_2 \\ \text{subject to } \partial_{\boldsymbol{n}} u_1 = \partial_{\boldsymbol{n}} u_2 = 0 \text{ on } \partial\Omega \end{cases} \tag{10}$$

Here $\mathcal{N}_l$ $(l = 1, 2)$ and $\mathcal{L}_{\mathrm{NL}}$ are the nonlinear partial differential operators and $g_l = 0$ $(l = 1, 2)$ is technical notation for numerical solutions that will be used in the next sections.

3 A nonlinear multigrid method

Full approximation scheme nonlinear multigrid (FAS-NMG) techniques [**?**, 17] have been prove to be very useful in image processing applications for solving large

systems of nonlinear equations arising from high-resolution digital images in real-life applications.

The basic idea of a FAS-NMG method is to smooth high frequency components of the error of the solution by performing a few steps with a so-called nonlinear smoother (an iterative relaxation technique) such that a smooth error term can be well represented and approximated on a coarser grid. After a nonlinear residual equation has been solved on the coarse grid, a coarse-grid correction is interpolated back to the fine grid and used to correct the fine grid approximation. Finally, the nonlinear smoother is performed again in order to remove some new high frequency components of the error introduced by the interpolation.

It is worth noticing that designing a suitable smoother is a major task in developing an efficient multigrid method. As already well known, the Newton-Gauss-Seidel relaxation do not perform well as a good smoother in leading to the convergence of the FAS-NMG technique for solving the nonlinear system related to the TV regularization technique. In this work, we then focus on designing a working smoother based on a typical FP method, which is *semi-implicit* in both regularizer and data terms. Staring with an initial guess $\boldsymbol{u}^{[0]}$ (e.g. $\boldsymbol{u}^{[0]} = 0$) leads to

$$\mathbf{N}[\boldsymbol{u}^{[\nu]}]\boldsymbol{u}^{[\nu+1]} = \mathbf{G}^{[\nu]}, \tag{11}$$

where $\boldsymbol{u}^{[\nu+1]} = (u_1^{[\nu+1]}, u_2^{[\nu+1]})^\top$, $\mathcal{L}_{\mathrm{NL}}^{\mathrm{lin}}[u_l^{[\nu]}]u_l^{[\nu+1]} = -\alpha\nabla\cdot(\frac{2\nabla u_l^{[\nu+1]}}{1+(\nabla \mathbf{u}_1^{[\nu]})^2})$, $G_l^{[\nu]} = g_l - f_l(u_1^{[\nu]}, u_2^{[\nu]})$,

$$\mathbf{N}[\boldsymbol{u}^{[\nu]}] = \begin{bmatrix} (\mathcal{L}_{\mathrm{NL}}^{\mathrm{lin}}[u_1^{[\nu]}] + \sigma_{11}^{[\nu]}) & \sigma_{12}^{[\nu]} \\ \sigma_{21}^{[\nu]} & (\mathcal{L}_{\mathrm{NL}}^{\mathrm{lin}}[u_2^{[\nu]}] + \sigma_{22}^{[\nu]}) \end{bmatrix},\ \mathbf{G}^{[\nu]} = \begin{pmatrix} G_1^{[\nu]} + \sigma_{11}^{[\nu]}u_1^{[\nu]} + \sigma_{12}^{[\nu]}u_2^{[\nu]} \\ G_2^{[\nu]} + \sigma_{22}^{[\nu]}u_2^{[\nu]} + \sigma_{21}^{[\nu]}u_1^{[\nu]} \end{pmatrix},$$

$$\sigma_{l1}^{[\nu]} = \partial_{u_1} f_l(u_1^{[\nu]}, u_2^{[\nu]}) = (\partial_{u_l} T(\boldsymbol{u}^{[\nu]}))(\partial_{u_1} T(\boldsymbol{u}^{[\nu]})) + (T(\boldsymbol{u}^{[\nu]}) - R)(\partial_{u_1 u_l} T(\boldsymbol{u}^{[\nu]})),$$

and

$$\sigma_{l2}^{[\nu]} = \partial_{u_2} f_l(u_1^{[\nu]}, u_2^{[\nu]}) = (\partial_{u_l} T(\boldsymbol{u}^{[\nu]}))(\partial_{u_2} T(\boldsymbol{u}^{[\nu]})) + (T(\boldsymbol{u}^{[\nu]}) - R)(\partial_{u_2 u_l} T(\boldsymbol{u}^{[\nu]})).$$

We note that the resulting linear system given by (11) can be solved by the so-called *block or pointwise collective Gauss-Seidel* (PCGS) relaxation method, i.e. all difference equations are updated simultaneously. In order to gain more

efficiency, one may introduce the so-called relaxation parameter $\omega \in (0, 2)$ and iterate the $\omega-$PCGS steps by

$$(\boldsymbol{u}^{[\nu+1]})_{i,j}^{(k+1)} = (1-\omega)\,(\boldsymbol{u}^{[\nu+1]})_{i,j}^{(k)} + \omega\underbrace{(\mathbf{N}[\boldsymbol{u}^{[\nu]}]_{i,j}^{(k+1)})^{-1}(\mathbf{G}^{[\nu]})_{i,j}^{(k+1/2)}}_{\text{original PCGS result}}. \tag{12}$$

We note further that the proposed smoother given by (12) shows the interaction between the actual FP iteration that overcomes the nonlinearity of the operator $\mathcal{N}_l$ at each outer step ν and the $\omega-$PCGS method that solves the resulting linear system of equations at each corresponding inner step k. Instead of solving the linear system of equations using the proposed smoother with very high precision, the smoother can perform only a *few iteration* to obtain an approximation solution at each outer step ν. This is likely the so-called *inexact lagged-diffusivity* method that have been widely used for solving other problems in image processing applications related to the TV regularization technique. We also note that line relaxation techniques, e.g. alternative line relaxation, are optional for the second step. However, we found with several numerical tests that they require less MG cycles in leading to the convergence of the FAS-NMG technique, but more computational costs than the proposed smoother given by (12). Finially, we note that in our FAS-NMG framework, the V-cycle is applied recursively down to the coarsest grid of a small number of grid points, typically 4×4. In order to compute the coarse-grid operator of $\mathcal{N}_l$, the so-called *discretization coarse grid approximation* (DCA) is used. For intergrid transfer operators between the fine- and coarse-grid domains, the averaging and bi-linear interpolation techniques are used for the restriction and interpolation operators; see the details in [17].

4 A robust approach for discontinuity-preserving image registration (RADPIR)

As is typical of Tikhonov regularization, the energy functional $\mathcal{J}_\alpha$ in (1) has a regularization parameter α. To provide well matched images, we have to carefully select α because it is in general unknown a priori. In order to find a suitable α automatically, we follow the 'cooling' process suggested in [2, 7] and references therein. The basic idea is to start with a high initial value of α and then slowly

reduce α such that the obtained solution can be used to be an excellent starting point for the next in order to decrease $\mathcal{J}_\alpha$. An alternative approach is to use a L-curve method.

Consider the discrete version of the minimization problem (1) with the same notation

$$\min \mathcal{J}_\alpha [\boldsymbol{u}] = \mathcal{D}(R, T(\boldsymbol{u})) + \alpha \mathcal{R}(\boldsymbol{u}). \tag{13}$$

Let α_1 be the initial value, which is sufficiently large. At the $(s+1)$th step we set $\alpha^{(s+1)} = \eta \alpha^{(s)} \in [\alpha_0, \alpha_1]$, where $\eta \in (0,1)$ is a constant, usually chosen to be about 0.5, and α_0 is a small positive number, e.g. 5×10^{-5}. Subsequently, we apply $\alpha^{(s+1)}$ and the initial guess solution obtained by the previous iteration $\boldsymbol{u}_{initial}^{(s+1)} = \boldsymbol{u}^{(s)}$ with the associated inner loop to obtain the optimal solution $\boldsymbol{u}^{(s+1)}$ within some tolerance. As mentioned in [2], since the functional $\mathcal{J}_\alpha$ is changing at each outer loop iteration, the demand of decreasing the value of the same functional is not reasonable. Then, the solution $\boldsymbol{u}^{(s+1)}$ and parameter $\alpha^{(s+1)}$ are acceptable if they satisfy the so-called *consistent condition*:

$$\mathcal{J}_{\alpha^{(s+1)}}[\boldsymbol{u}^{(s+1)}] = \mathcal{D}[\boldsymbol{u}^{(s+1)}] + \alpha^{(s+1)} \mathcal{R}[\boldsymbol{u}^{(s+1)}] < \mathcal{J}_{\alpha^{(s+1)}}[\boldsymbol{u}^{(s)}] = \mathcal{D}[\boldsymbol{u}^{(s)}] + \alpha^{(s+1)} \mathcal{R}[\boldsymbol{u}^{(s)}].$$

However, if this condition is not satisfied, we increase η (usually to 0.9) and re-start the step. Our experience suggests that the stopping criterion given by

$$\frac{\left\| \boldsymbol{u}^{(s+1)} - \boldsymbol{u}^{(s)} \right\|_{l_2}}{\max\{ \left\| \boldsymbol{u}^{(s+1)} \right\|_{l_2}, \left\| \boldsymbol{u}^{(s)} \right\|_{l_2} \}} < \delta \tag{14}$$

is suitable, where $\delta > 0$ is small (normally set to 10^{-3}).

In order to save computational work for high-resolution digital images, a low-tolerance is applied to reduce the accumulated costs in each minimization problem solved by our FAS-NMG method and we shall name this method by *a robust approach for discontinuity-preserving image registration* (RADPIR). In order to increase the performance of this method, we propose to use a hierarchy of L grids (with level L the finest and level 1 the coarsest one) with the so-called *multi-resolution* or *multilevel continuation technique*. Firstly we shall seek the optimal α on the coarsest level 1 with the grid size of 32×32 only (we selected this size of grid points because it still contains useful information from the low-resolution

versions of the given images) and secondly we use the multilevel continuation idea to provide the initial guesses for the next finer level while using our FAS-NMG method.

5 Numerical examples

In this section we demonstrate 3 sets of experiments results

- the abilities of $\mathcal{R}^{\mathrm{MTV}}$ in solving the particular registration problems as represented by Example 1[1]-2[2] shown respectively in Figure 1 (a)-(b) and Figure 3 (a)-(b);
- the overall performance of our proposed numerical methods on a set of medical data by processing Example 2 shown in Figure 3 (a)-(b);
- a comparison between our FAS-NMG method and the semi-implicit time marching schemes on the set of clinical images in Example 2.

In all experiments, the bi-linear interpolation technique was used to compute $T(\boldsymbol{u})$, and $\nu_1 = 5$, $\nu_2 = 5$, $\omega = 1.85$, $GSiter = 5$ (the $\omega-$PCGS steps) were employed in the multigrid procedure with a zero deformation field as initialization. For medical images we preprocessed them with a Gaussian kernel of standard deviation $\widehat{\sigma} = 1$.

5.1 Comparison $\mathcal{R}^{\mathbf{MTV}}$ with different regularization techniques

In this experiment, our aim is to investigate capabilities of $\mathcal{R}^{\mathrm{MTV}}$, $\mathcal{R}^{\beta\mathrm{TV}}$ and $\mathcal{R}^{\mathrm{diff}}$, which belong to the same class of variational image registration models using 1^{st}-order partial derivatives, in solving Example 1-2. To be a fair comparison, we used the same systematic formulation as explained in Sections 3-4 for solving the discretised Euler-Lagrange equations related to $\mathcal{R}^{\beta\mathrm{TV}}$ and $\mathcal{R}^{\mathrm{diff}}$.

As shown in Figure 1 (c)-(e), on one hand, $\mathcal{R}^{\mathrm{MTV}}$ and $\mathcal{R}^{\beta\mathrm{TV}}$ produced visually pleasing registration results, while $\mathcal{R}^{\mathrm{diff}}$ did not. The main reason is that the exact deformation field is given by a shift of the upper rectangular to the right and a shift of the lower rectangular to the left; c.f. Figure 2 (a)-(b). Therefore, the exact

[1] Adapted from [5]
[2] Source: http://www.math.mu-luebeck.de/safir/

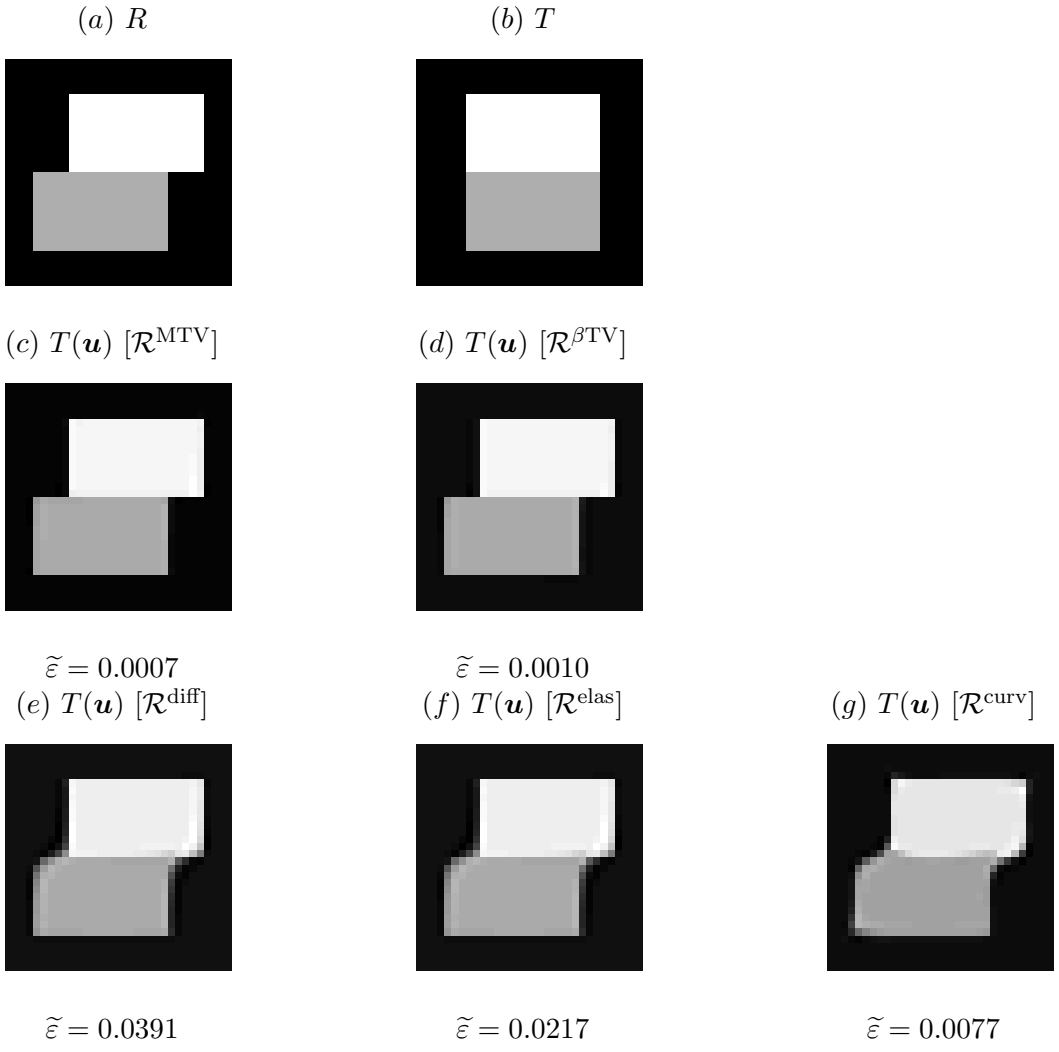

Figure 1: Registered images for two rectangular blocks shown in (a) R and (b) T of size 32×32 (Example 1): results by (c) $\mathcal{R}^{\mathrm{MTV}}$, (d) $\mathcal{R}^{\beta\mathrm{TV}}$ with $\beta = 0.0001$, (e) $\mathcal{R}^{\mathrm{diff}}$, (f) $\mathcal{R}^{\mathrm{elas}}$ with $(\mu, \lambda) = (1, 0)$, and (g) $\mathcal{R}^{\mathrm{curv}}$. Recall that $\widetilde{\varepsilon}_3$ means the relative reduction of dissimilarity.

deformation field is piecewise constant with substantial discontinuities at regions close to the interface between the upper and the lower rectangular. Consequently, $\mathcal{R}^{\mathrm{diff}}$ must fail because it tries to smooth the deformation field as much as possible at those regions; see over smoothing results of the field as shown in Figure 2 (c). On the other hand, as shown in Figures 4 (a)-(c) $\mathcal{R}^{\mathrm{MTV}}$ and $\mathcal{R}^{\mathrm{diff}}$ gave slightly better registration results than those of $\mathcal{R}^{\beta\mathrm{TV}}$ in terms of $\widetilde{\varepsilon}$ (the relative reduction of dissimilarity), but the corresponding deformation fields shown in Figures 5 (b)-(c) are more reasonable than that of $\mathcal{R}^{\beta\mathrm{TV}}$ depicted in Figures 5 (a). This because the exact deformation field is globally smooth, almost the same shapes as determined

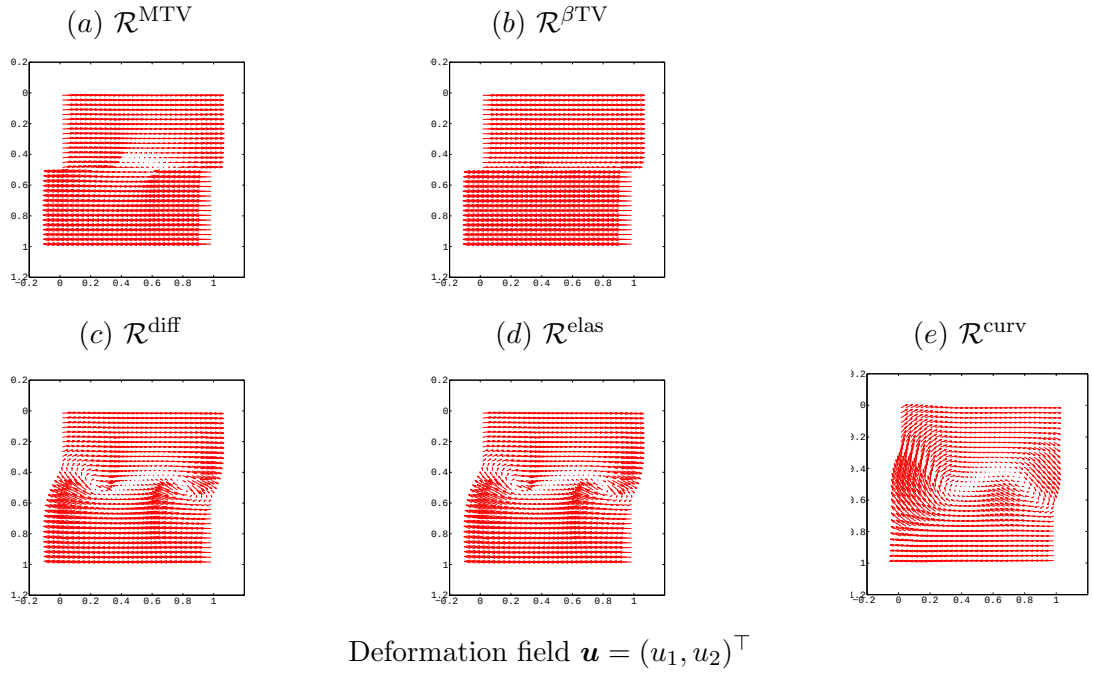

Figure 2: Deformation fields for the registration problem shown in Figure 1 (a)-(b) (Example 1): results by (a) $\mathcal{R}^{\mathrm{MTV}}$, (b) $\mathcal{R}^{\beta\mathrm{TV}}$ with $\beta = 0.0001$, (c) $\mathcal{R}^{\mathrm{diff}}$, (d) $\mathcal{R}^{\mathrm{elas}}$ with $(\mu, \lambda) = (1, 0)$, and (e) $\mathcal{R}^{\mathrm{curv}}$.

by $\mathcal{R}^{\mathrm{MTV}}$ and $\mathcal{R}^{\mathrm{diff}}$, but the results of $\mathcal{R}^{\beta\mathrm{TV}}$ are almost piecewise constant in some parts of the upper regions. Both experiments confirm that $\mathcal{R}^{\mathrm{MTV}}$ is a half way between $\mathcal{R}^{\beta\mathrm{TV}}$ and $\mathcal{R}^{\mathrm{diff}}$. In other words, $\mathcal{R}^{\mathrm{MTV}}$ is compatible with $\mathcal{R}^{\beta\mathrm{TV}}$ for registration problems requiring to preserve discontinuities and it is compatible with $\mathcal{R}^{\mathrm{diff}}$ for those registration problems requiring to have global smoothness of the field. In case of $\mathcal{R}^{\mathrm{elas}}$ and $\mathcal{R}^{\mathrm{curv}}$, we found by applying different numerical techniques given in [15] that registration results are similar to those of $\mathcal{R}^{\mathrm{diff}}$ as shown in Figures 1 (f)-(g), 2 (d)-(e), 4 (d)-(e), and 5 (d)-(e).

5.2 $h-$independent convergence tests

One of the key properties of multigrid techniques is that their convergence does not depend on the number of grid points. Thus, in the second test we designed our experiments on clinical images by processing Example 2 as shown in Figure 3. The number of multigrid steps (V-cycles) used to drop the relative residual below 10^{-8}, the relative reduction of dissimilarity, and the runtimes (in seconds) are given in Table 1 with different sizes of grid points. The results show that all registration algorithms not only converge within a few multigrid steps as expected

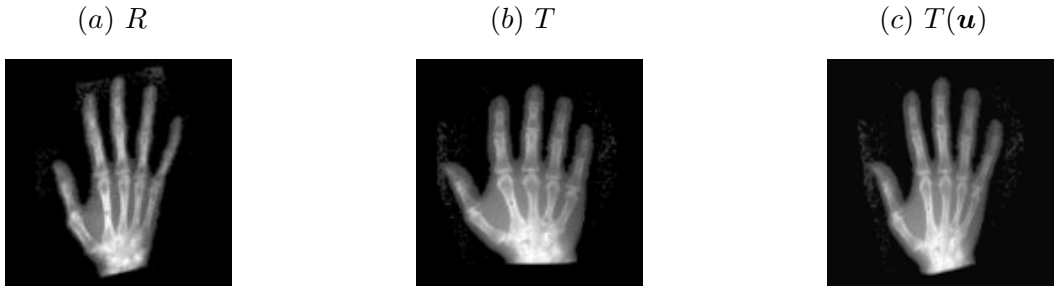

Figure 3: Registration results for X-ray and MRI images (Examples 2 (a)-(b)) using the proposed numerical methods. Left column: reference R, center column: template T, right column: the deformed template image $T(\boldsymbol{u})$ obtained from $\mathcal{R}^{\mathrm{MTV}}$.

from a multigrid technique, but they are also accurate because the dissimilarities between the reference and registered images have been reduced more than 88%. For overall performance the experimental results suggest that the multilevel RADPIR method would be preferred for practical applications because the multi-resolution idea used in cooling α has been prove to be very useful for initialization. It results in speeding up overall runtimes of the standard RADPIR method around 3 times.

	FAS-NMG N/R/D/C	**RADPIR** N/R/D/IC/C	**Multilevel+RADPIR** N/R/D/IC/C
Example 2 :	$\alpha = 0.0909$		
$h = 1/128$	$8/3.1 \times 10^{-9}/0.1012/26.2$	$4/6.6 \times 10^{-9}/0.0917/95.4/110.1$	$6/7.1 \times 10^{-9}/0.0917/21.6/41.0$
$h = 1/256$	$8/1.8 \times 10^{-9}/0.1098/134.4$	$5/3.6 \times 10^{-9}/0.1098/298.0/365.1$	$6/3.1 \times 10^{-9}/0.1098/29.4/109.5$
$h = 1/512$	$8/9.5 \times 10^{-9}/0.1150/453.3$	$5/1.4 \times 10^{-9}/0.1124/1402.1/1707.5$	$6/4.4 \times 10^{-9}/0.1124/57.9/396.1$
$h = 1/1024$	$8/3.6 \times 10^{-9}/0.1168/1864.4$	$5/2.1 \times 10^{-9}/0.1168/5137.5/6289.7$	$5/6.5 \times 10^{-9}/0.1168/171.9/1332.1$

Table 1: Registration results of the proposed numerical methods for processing Examples 2 shown in Figure 3 (a)-(b). The letters 'N', 'R', 'D', 'C', and 'IC' mean the number of multigrid steps, the relative reduction of residual, the relative reduction of dissimilarity, the total runtimes, and the initial runtimes for determining the optimal α and initial guess $\boldsymbol{u}^{(0)}$, respectively.

5.3 Comparison our FAS-NMG method with the semi-implicit time-marching schemes

The main aim of this experiment is to show that the parabolic approaches are quite slow in achieving convergence. We took Example 2 to illustrate this point. Table 2 summarizes the results for the standard semi-implicit and additive operator splitting (AOS) time marching schemes with different numbers of grid points. To be a fair comparison between them, we used those results determined by our FAS-

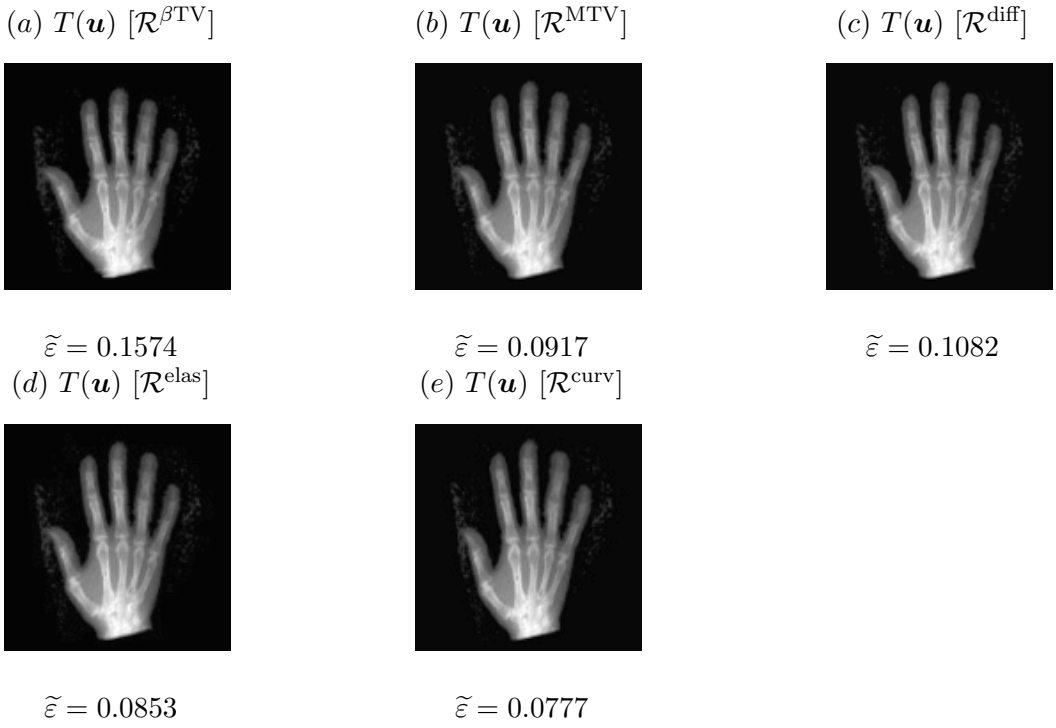

Figure 4: Registration results for the problem of size 128×128 shown in Figure 3 (a)-(b) (Example 2): results by (a) $\mathcal{R}^{\beta\mathrm{TV}}$ with $\beta = 0.001$, (b) $\mathcal{R}^{\mathrm{MTV}}$, (c) $\mathcal{R}^{\mathrm{diff}}$, (d) $\mathcal{R}^{\mathrm{elas}}$ with $(\mu, \lambda) = (1, 0)$, and (e) $\mathcal{R}^{\mathrm{curv}}$.

NMG method represented in Table 1. That is, we started all methods with the same $\alpha = 0.0909$ and the same initial guess, $\boldsymbol{u}^{(0)} = 0$. Here, the time-step τ is required to be sufficiently small for each size of the problem. We used $\tau = 10^{-4}$ for $h = 1/128 - 1/512$ and $\tau = 10^{-6}$ for $h = 1/1024$. As expected from the experiments, all methods are accurate in registering the given images because the dissimilarities between the reference and registered images have been reduced more than 88%. However both time marching methods fail to drop the relative residual to 10^{-8} in a few time steps (even large values of τ are used) and the runtimes used by our FAS-NMG method are significantly faster in delivering the same level of the relative dissimilarity.

6 Conclusions

In this paper, we have proposed first a novel regularization technique, a half way between diffusion and TV regularization techniques, for deformable image registration, and then a fully automatic, fast, and accurate approach based on the

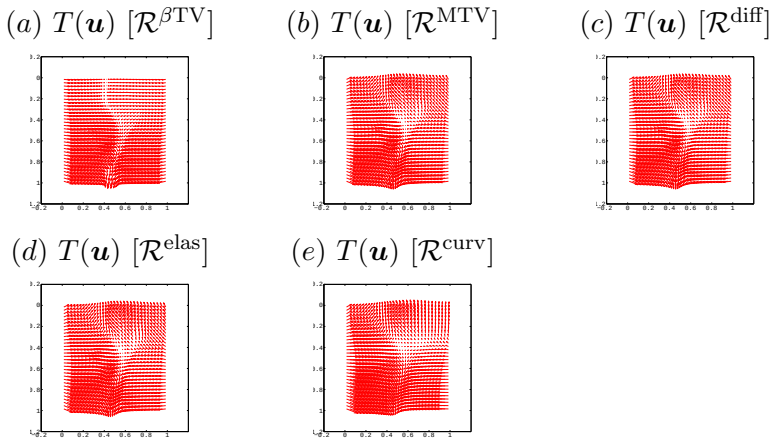

Figure 5: Deformation fields for the registration problem shown in Figure 3 (a)-(b) (Example 2): results by (a) $\mathcal{R}^{\beta\mathrm{TV}}$ with $\beta = 0.001$, (b) $\mathcal{R}^{\mathrm{MTV}}$, (c) $\mathcal{R}^{\mathrm{diff}}$, (d) $\mathcal{R}^{\mathrm{elas}}$ with $(\mu, \lambda) = (1, 0)$, and (e) $\mathcal{R}^{\mathrm{curv}}$.

	Standard Semi-Implicit N/R/D/C	**AOS** N/R/D/C
$h = 1/128$	21973/ $*$ /0.1012/5232.4 (1.45 hours)	23946/ $*$ /0.1012/3074.1 (0.85 hours)
$h = 1/256$	19808/ $*$ /0.1098/25513.9 (7.08 hours)	21197/ $*$ /0.1098/15587.0 (4.32 hours)
$h = 1/512$	$*$/ $*$ / $*$ /$*$ (> 15 hours)	16637/ $*$ /0.1150/53757.1 (14.9 hours)
$h = 1/1024$	$*$/ $*$ / $*$ /$*$ (> 15 hours)	$*$/ $*$ / $*$ /$*$ (> 15 hours)

Table 2: Registration results of the proposed FAS-NMG method, the standard semi-implicit, and AOS time marching methods for Example 2 shown in Figure 3 (a)-(b). $*$ indicates either computation stopped after about 15 hours or failure in dropping the relative residual to 10^{-8}.

FAS-NMG strategy and the automatic procedure in selecting the optimal value of α for solving the corresponding variational problem. Numerical tests confirm that the proposed regularization technique is more flexible than those common techniques such as the diffusion and total variation based regularization techniques. They also show that the FAS-NMG technique based on the proposed smoother is $h-$independent convergence and much faster than those of semi-implicit time-marching schemes in delivering the same numerical results. Future works will address a typical regularization technique and multigrid methods of other regularization techniques for deformable image registration, and in particular 3D problems.

References

[1] G. Aubert, and P. Kornprobst, *Mathematical Problems in Image Processing: Partial Differential Equations and the Calculus of Variations*, Second ed., Springer (2006).

[2] N. Chumchob, and K. Chen, *A Multigrid Approach Based on a Robust Smoother for Diffusion Image Registration*, Submitted (2009).

[3] B. Fischer, and J. Modersitzki, *Fast diffusion registration*, in: "Inverse problems, image analysis, and medical imaging; proceedings. (Contemporary mathematics series; No.313 (2002))", eds. M.Z. Nashed, O. Scherzer, 117-129.

[4] B. Fischer, and J. Modersitzki, *Curvature Based Image Registration*, Journal of Mathematical Imaging and Vision, Vol. **18** (2003), 81 - 85.

[5] C. Frohn-Schauf, S. Henn, and K. Witsch, *Multigrid based total variation image registration*, Comput. Visual. Sci., Vol. **11** (2008), 101-113.

[6] S. Gao, L. Zhang, H. Wang, R. de Crevoisier, D.D. Kuban, R. Mohan, and L. Dong, *A deformable image registration method to handle distended rectums in prostate cancer radiotherapy*, Med. Phys., Vol. **33** No. **9** (2006), 3304-3312.

[7] E. Haber, and J. Modersitzki, *A multilevel method for image registration*, SIAM J. Sci. Comput., Vol. **27** No. **5** (2006), 1594-1607.

[8] S. Henn, and K. Witsch, *Iterative multigrid regularization techniques for image matching*, SIAM J. Sci. Comput., Vol. **23** No. **4** (2001), 1077-1093.

[9] S. Henn, *A Multigrid Method for a Fourth-Order Diffusion Equation with Application to Image Processing*, SIAM J. Sci. Comput., Vol. **27** No. **3** (2005), 831-849.

[10] L. Hömke, *A multigrid method for anisotropic PDEs in elastic image registration*, Numer. Linear Algebra Appl., Vol. **13** (2006), 215-229.

[11] H. Köstler, K. Ruhnau, and R. Wienands, *Multigrid solution of the optical flow system using a combined diffusion- and curvature-based regularizer*, Numer. Linear Algebra Appl., Vol. **15** (2008), 201-218.

[12] J. Larrey-Ruiz, R. Verdú-Monedero, and J. Morales-Sánchez, *A Fourier Domain Framework for Variational Image Registration*, Journal of Mathematical Imaging and Vision, Vol. **32** (2008), 57-72.

[13] W. Lu, M.L. Chen, G.H. Olivera, K.J. Ruchala, and T.R. Mackie, *Fast free-form deformable registration via calculus of variations*, Phys. Med. Biol. **49** (2004), 3067-3087.

[14] J.B.A. Maintz, and M.A. Viergever, *A survey of medical image registration*, Med. Image. Anal., Vol. **2** No. **1** (1998), 1-36.

[15] J. Modersitzki, *Numerical Methods for Image Registration*, Oxford (2004).

[16] L. Rudin, S. Osher, and E. Fatemi, *Nonlinear total variation based noise removal algorithms*, Phys.D, Vol. **60** (1992), 259-268.

[17] U. Trottenberg, C. Oosterlee, and A. Schuller, *Multigrid*, Academic Press (2001).

[18] M. Stürmer, H. Köstler, and U. Rüde, *A fast full multigrid solver for applications in image processing*, Numer. Linear Algebra with Appl., Vol. **15** (2008), 187-200.

[19] D. Zikic, W. Wein, and A. Khamene, *Fast Deformable Registration of 3D-Ultrasound Data Using a Variational Approach*, LNCS **4190** (2006), 915-923.